

A Neuron-Based Screening Platform for Optimizing Genetically-Encoded Calcium Indicators

Trevor J. Wardill¹✉, Tsai-Wen Chen¹✉, Eric R. Schreiter¹, Jeremy P. Hasseman¹, Getahun Tsegaye¹, Benjamin F. Fosque¹, Reza Behnam², Brenda C. Shields², Melissa Ramirez², Bruce E. Kimmel¹, Rex A. Kerr¹, Vivek Jayaraman¹, Loren L. Looger¹, Karel Svoboda¹, Douglas S. Kim^{1*}

1 Genetically-Encoded Neuronal Indicator and Effector Project, Janelia Farm Research Campus, Howard Hughes Medical Institute, Ashburn, Virginia, United States of America, **2** Janelia Farm Research Campus, Howard Hughes Medical Institute, Ashburn, Virginia, United States of America

Abstract

Fluorescent protein-based sensors for detecting neuronal activity have been developed largely based on non-neuronal screening systems. However, the dynamics of neuronal state variables (e.g., voltage, calcium, etc.) are typically very rapid compared to those of non-excitabile cells. We developed an electrical stimulation and fluorescence imaging platform based on dissociated rat primary neuronal cultures. We describe its use in testing genetically-encoded calcium indicators (GECIs). Efficient neuronal GECI expression was achieved using lentiviruses containing a neuronal-selective gene promoter. Action potentials (APs) and thus neuronal calcium levels were quantitatively controlled by electrical field stimulation, and fluorescence images were recorded. Images were segmented to extract fluorescence signals corresponding to individual GECI-expressing neurons, which improved sensitivity over full-field measurements. We demonstrate the superiority of screening GECIs in neurons compared with solution measurements. Neuronal screening was useful for efficient identification of variants with both improved response kinetics and high signal amplitudes. This platform can be used to screen many types of sensors with cellular resolution under realistic conditions where neuronal state variables are in relevant ranges with respect to timing and amplitude.

Citation: Wardill TJ, Chen T-W, Schreiter ER, Hasseman JP, Tsegaye G, et al. (2013) A Neuron-Based Screening Platform for Optimizing Genetically-Encoded Calcium Indicators. PLoS ONE 8(10): e77728. doi:10.1371/journal.pone.0077728

Editor: Xiangming Zha, University of South Alabama, United States of America

Received: March 1, 2013; **Accepted:** September 4, 2013; **Published:** October 14, 2013

Copyright: © 2013 Wardill et al. This is an open-access article distributed under the terms of the Creative Commons Attribution License, which permits unrestricted use, distribution, and reproduction in any medium, provided the original author and source are credited.

Funding: This work was supported by funding from the Howard Hughes Medical Institute. The funders had no role in study design, data collection and analysis, decision to publish, or preparation of the manuscript.

Competing interests: The authors have the following competing interests. A patent application has been filed on the neuronal culture screening methods ("Genetically Encoded Calcium Indicators and Methods of Use" USPTO 61/711,995). There are no further patents, products in development or marketed products to declare. This does not alter the authors' adherence to all the PLOS ONE policies on sharing data and materials, as detailed online in the guide for authors.

* E-mail: kimd@janelia.hhmi.org

✉ These authors contributed equally to this work.

✉ Current address: Program in Sensory Physiology and Behavior, Marine Biological Laboratory, Woods Hole, Massachusetts, United States of America

Introduction

Fluorescent protein-based sensors of neuronal activity are beginning to revolutionize neurophysiology [1]. Protein sensors enable *in vivo* recording of hundreds of neurons simultaneously [2] over chronic timescales [3–5]. Protein sensors also facilitate measurements of excitation in tiny neurons [6] and neuronal microcompartments, such as dendritic spines [7] and axonal terminals [8,9], which are inaccessible to electrophysiological methods. Protein sensors can be targeted to specific neuron types using gene regulatory elements [10]. They can thus be delivered to cells of interest in a non-invasive manner [11,12].

The optimization of sensors for neuronal activity would greatly benefit from testing in neuronal systems. Neurons

[13,14] and neuronal microcompartments [15,16] have unusually small and fast calcium dynamics, which are difficult to model in non-excitabile cells [17]. Previous efforts in engineering sensors have tested candidates in non-neuronal assays, including assays using purified proteins and tissue culture cells [5,18–20]. Other efforts have tested sensors in lower throughput *in vitro* and *in vivo* systems, such as rat neuronal slice cultures, fly neurons, and fish neurons [7,21–24].

Recently, a high-throughput stimulation and imaging system for neurons has been developed for drug screening using an indicator of synaptic function [25]. Here we combine a similar system with high-resolution imaging, suitable to assess the millisecond timescale dynamics of sensors in individual neurons. This allows us to screen sensors under physiological

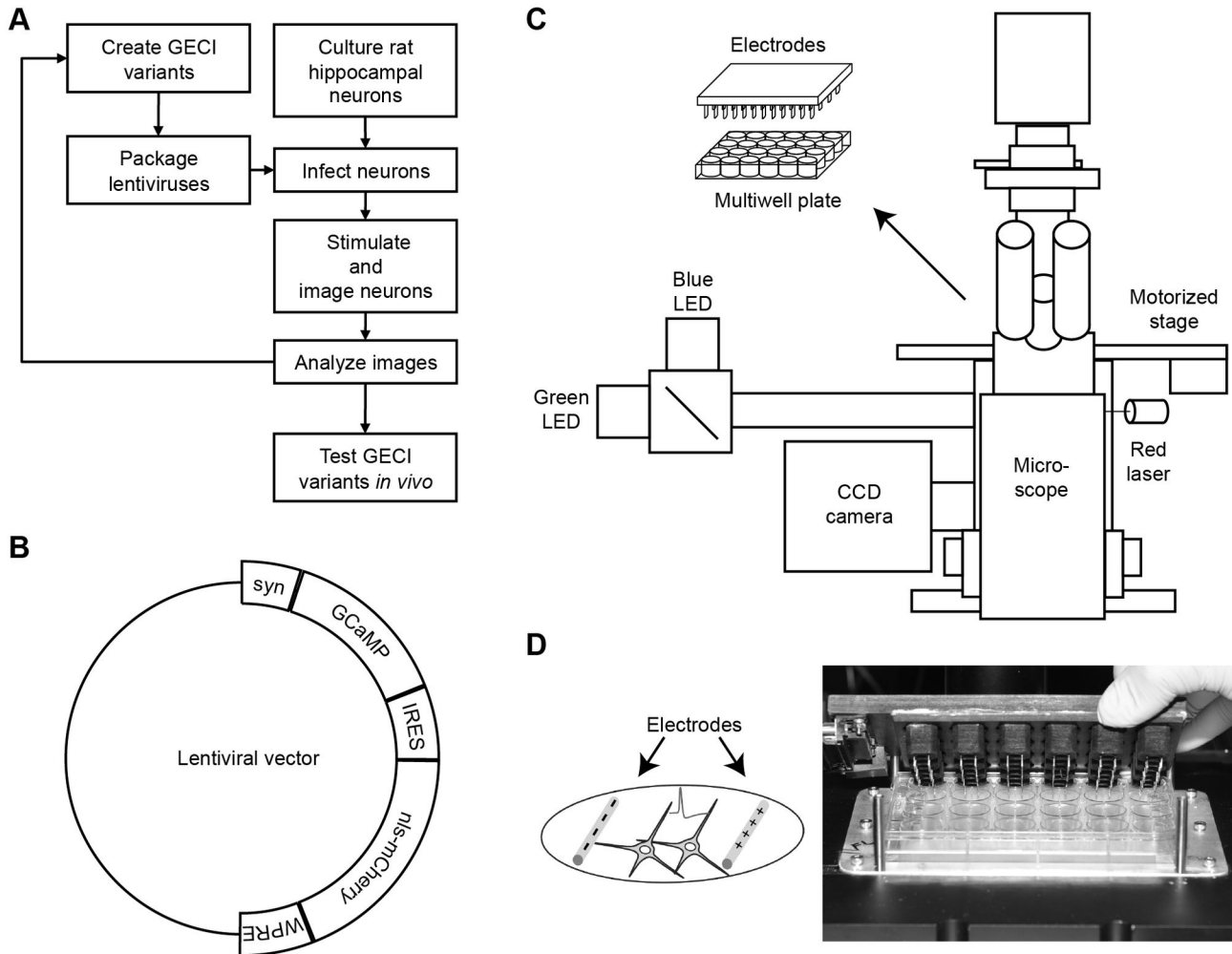


Figure 1. Primary neuron stimulus and imaging screening platform. (A) Flow chart for GECI optimization on screening platform. (B) Pro-lentiviral vector with human *synapsin-1* promoter (syn), GCaMP variant, internal ribosome entry site (IRES), nuclear localization signal fused with mCherry (nls-mCherry), and woodchuck hepatitis virus post-transcriptional regulatory element (WPRE). (C) Schematic of screening platform. (D) Schematic of electrodes evoking APs from cultured neurons. Photo of 24-well cap stimulator with pairs of parallel platinum wires.

doi: 10.1371/journal.pone.0077728.g001

conditions. We tested this platform by assaying performance of GECI variants.

Results

Indicator expression in neuronal cultures on screening platform

We developed a neuron-based platform to screen activity indicators (Figure 1). We evaluated the capabilities of this novel screening platform by expressing and imaging of variants of the green fluorescent GECI, GCaMP3 [5]. GCaMP detects calcium increases via a calcium-dependent calmodulin and M13 peptide interaction that modulates the chromophore environment of a tethered GFP domain and augments fluorescence. Protein variants were made by mutating the

GCaMP3 coding region using site-directed mutagenesis at selected positions in a lentiviral expression vector (Figure 1B). The large size of the lentiviral vector and the presence of recombinogenic repeat sequences made whole plasmid PCR-based mutagenesis difficult. Mutagenesis was instead carried out by mutation of coding regions and subsequent sequence assembly with the lentiviral vector.

Individual variants were packaged in lentiviral particles in tissue culture cells. Dissociated neonatal rat hippocampal cells were then infected at 3 days *in vitro* in 24-well, glass-bottom plates for 18 hours, with unconcentrated viral particles. Glial proliferation was inhibited on day 4 by addition of the nucleoside analogue, AraC. Neuron-selective expression was achieved using a 476-bp human *synapsin-1* promoter element [26]. Additionally, a nuclear localization signal (nls) tagged red

fluorescent protein was co-expressed in neurons using an internal ribosome entry site (IRES)-nls-mCherry sequence (Figure 1B) [27]. Red fluorescence was used both for image segmentation and measurement of relative GCaMP expression across cells. Hippocampal cultures included excitatory glutamatergic and inhibitory GABAergic neurons (data not shown).

Electrical field stimulation and fluorescence imaging

At 16–18 days *in vitro*, GCaMP expression reached sufficient levels for imaging, and neurons were capable of firing trains of APs [28]. GCaMP variants were tested on the platform (Figure 1C) by measuring fluorescence changes in response to field stimulation of neuronal cultures. Growth medium was exchanged with imaging buffer. Neuronal culture wells were stimulated using a custom-built 24-well cap stimulator (Figure 1D). Each well contained a pair of parallel platinum wires, and each pair could be independently controlled. Wells were illuminated by LEDs, and images were captured using an EMCCD camera. A motorized microscope stage allowed automated image acquisition from multiple wells in sequence (Figure 1C).

Fields of view (800 μm \times 800 μm) were located from a predetermined list of stage coordinates, corresponding to centers of each well. Imaging and stage movement were controlled by MetaMorph software (Molecular Devices). The variation in the glass bottom of wells ranged up to 500 μm in z position across a plate, which made well-by-well focusing necessary. An imaging-based autofocus routine, based on computing nearest neighbor pixel contrast in the mCherry channel [29], was used. After focusing, reference mCherry, GCaMP, and bright field images were acquired.

A trigger (provided by MetaMorph) simultaneously initiated imaging and field stimulation. Electrical stimulation parameters were controlled as a slave by a separate custom software package (Ephus) [30]. Image timing data from the camera, temperature from thermocouples, LED light levels, stimulus current, and stimulus voltage were recorded at 10 kHz. Buffer temperature was $\sim 30^\circ\text{C}$. Fluorescence image streams (35 frames/s, 250 frames) were captured using a cooled EMCCD camera controlled by MetaMorph.

Image segmentation and analysis

To assay GECI performance at cellular resolution, we identified regions of interest corresponding to nls-mCherry- and GCaMP-positive neuronal cell bodies using custom software. To define regions of interest, a raw mCherry image was low-pass filtered with a circular kernel roughly the size of a cell nucleus (Figure 2A,B). Putative locations of cells were determined as the local maxima of the filtered image whose intensity crossed an adaptively defined threshold. Based on these seed locations, a Voronoi diagram was drawn to cut the image into multiple sub-regions (Figure 2C) [31]. Adaptive thresholding was performed on the GCaMP and mCherry image within each sub-region to define pixels belonging to the cytosolic and nuclear regions of interest, respectively (Figure 2D). Averaged baseline GCaMP and mCherry fluorescence was measured within each cytosolic or nuclear region of

interest, and cells were excluded if the average mCherry level did not reach a predefined threshold (Figure 2E). Regions of interest that touched the boundary of the image were also excluded as a further quality control. Segmentation increased the sensitivity of the assay by narrowing regions of interest to exclude extraneous background (Figure 2F). The median peak $\Delta F/F_0$ (change in fluorescence normalized by initial fluorescence) response of GCaMP3 to 10 AP stimulus increased from $31.6 \pm 4.1\%$ to $70.7 \pm 5.9\%$ after segmentation (median \pm s.e.m.; Student's paired t-test, $p=1.6 \times 10^{-12}$). Responses were also less variable because segmentation excluded inactive pixels, which varied in number from well to well. The coefficient of variation decreased from 62.8% to 46.6% after segmentation.

Examples of evoked GCaMP3 $\Delta F/F_0$ responses under optimized stimulation conditions and with glutamate and GABA receptor blockers in the imaging buffer (see further below) are shown in Figure 3A,B,C. Fluorescence traces from segmented neuronal cell bodies over time exhibited variable $\Delta F/F_0$ responses across different regions of interest (Figure 3D,E,F). Possible sources of neuron-to-neuron variability included neuronal subtype diversity, differential electrical stimulation, connectivity differences, and variations in segmentation accuracy.

Stimulus parameters for action potential generation

Stimulus parameters were optimized for AP generation using GCaMP3 by varying field pulse (FP) voltage, frequency, and width [9,32]. In terms of voltage, frequency, and pulse width, the average $\Delta F/F_0$ response to 10 FP in segmented neuronal cell bodies reached an absolute maximum at 30 V, 83 Hz, and 500 μs , respectively (Figure 4A,B,C). The response remained stable from the same well even after delivering 15 trains spaced ~ 1 min apart of 10 field pulses at 40 V, 83 Hz, and 1 ms pulse width (Figure 4D). Additionally, the first and last replicate wells of GCaMP3-expressing neurons on plates responded within similar ranges, indicating that neurons remained healthy throughout the assay period (Figure 4E). Based on these results, parameters were fixed at 40 V, 83 Hz, and 1 ms width to ensure suprathreshold stimulation. Calcium responses evoked by these stimulus conditions were dependent on stimulator evoked APs (Figure 4F). The calcium response of neurons loaded with the synthetic calcium dye, Fluo4, was completely and reversibly abolished by blocking voltage-gated sodium channels with tetrodotoxin. To further confirm that APs were evoked, we also measured membrane potentials using the archaerhodopsin-3-based voltage sensor (ArchWT-GFP; Figure 4G,H) [33]. Red laser illumination (638 nm, ~ 500 W/cm²; Figure 1C) and a high-speed EMCCD camera (500 frame/s) were used. With 40 V, 83 Hz, and 1 ms stimulus parameters, 10 FP evoked 10 AP (Figure 4G,H, Figure S1). Subthreshold depolarizations were observed with submaximal field stimulation (Figure S1). In screening, stimulus trains of 1, 2, 3, 5, 10, 20, 40, 80, and 160 AP were delivered with an intrastimulus interval of ~ 20 s. These trains were chosen to assess GCaMP performance over the full dynamic range of these cultured hippocampal neurons. Stimulus order was kept constant for screening.

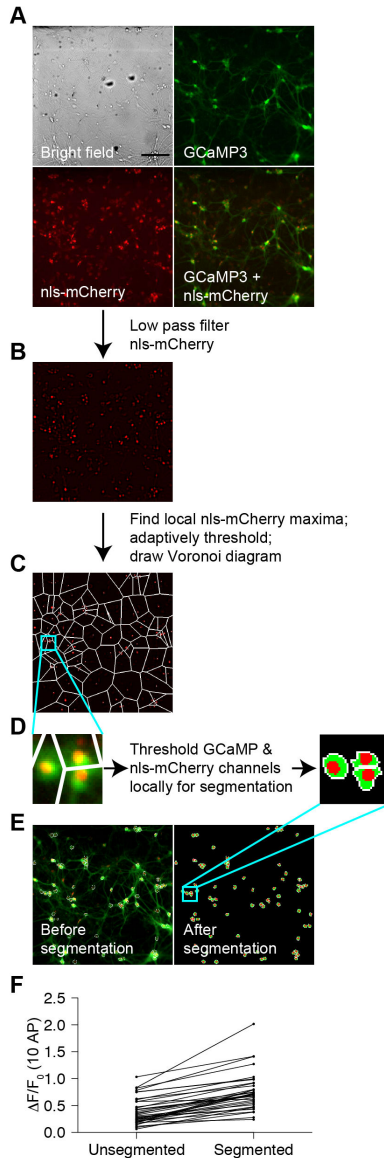


Figure 2. Segmentation of neuronal cell bodies for image analysis. (A) Bright field and epifluorescence images showing GCaMP3 fluorescence channel, nls-mCherry fluorescence channel, and red and green merged fluorescence channels. Scale bar: 150 μ m. (B) nls-mCherry fluorescence channel after low-pass frequency filtering with a circular kernel to identify putative nuclei. (C) Partially segmented image where local intensity maxima were identified using adaptively defined thresholds followed by cutting of image into a Voronoi diagram based on seeds identified by maxima. (D) Images from inset in (C) before and after adaptive thresholding in the GCaMP and mCherry channels within each sub-region to define pixels that belong to cytosol and nuclei. (E) Images before and after final segmentation, where regions of interest were excluded if the average mCherry level did not reach a predefined threshold or if the regions of interest touched the image boundary. (F) GCaMP3 10 AP $\Delta F/F_0$ response before and after segmentation (36 wells).

doi: 10.1371/journal.pone.0077728.g002

Control of calcium response amplitude and variability with glutamate and GABA receptor blockers

Neuronal cultures formed functional networks. To control for network variability across wells, we sought to isolate individual neuronal responses from network influences by using neurotransmitter receptor inhibitors, including AMPA and NMDA glutamatergic receptors blockers CNQX and CPP (10 μ M; Figure 5A). Without these antagonists, the variability and magnitude of responses were relatively large (Figure 5A, inset), likely reflecting variable recurrent excitation in networks formed in culture. Consistent with the presence of inhibitory GABAergic neurons, addition of a GABA_A receptor antagonist, gabazine (10 μ M), disinhibited the GCaMP3 response, doubling the $\Delta F/F_0$ for 10 AP stimulus (Figure 5A). A slow component of the GCaMP3 response was blocked by MCPG (1 mM). This metabotropic glutamate receptor blocker can inhibit G_q-mediated activation of intracellular calcium release. CNQX, CPP, gabazine, and MCPG were thus used together in screening to dampen variability due to network effects and intracellular calcium release and increase calcium response amplitudes over those obtained with vehicle (Figure 5B).

Neuron-based screening platform performance

We evaluated platform performance using the GCaMP3 construct. Nuclear mCherry fluorescence levels were correlated with GCaMP3 basal fluorescence (Figure 6A; linear regression, $R^2=0.38$, $F(1,247)=153.1$, $p<2.2 \times 10^{-16}$). In screening, mCherry was thus used to normalize basal fluorescence values for GCaMP3 variants with variable F_0 related to mutations. The $\Delta F/F_0$ response to 10 AP was weakly and inversely related to GCaMP3 expression levels, estimated by mCherry fluorescence (Figure 6B; linear regression, $R^2=0.08$, $F(1,247)=21.52$, $p=5.68 \times 10^{-6}$). Higher expression levels might have resulted from a greater multiplicity of viral infection in wells with fewer neurons. Consistent with this notion, mCherry fluorescence was inversely correlated with the number of infected cells (Figure 6C; linear regression, $R^2=0.07$, $F(1,247)=17.44$, $p=4.11 \times 10^{-5}$). Additionally, the GCaMP3 response of neurons was correlated with the number of infected neurons (Figure 6D; linear regression, $R^2=0.31$, $F(1,247)=109.9$, $p<2.2 \times 10^{-16}$), perhaps reflecting less calcium buffering by GCaMP3 with lower expression in higher density wells. This relationship was used to correct for response variability (see below). Clumping of neurons in wells was associated with markedly increased $\Delta F/F_0$ GCaMP3 responses in the low AP range (Figure S2). In wells with clumped neurons, the GCaMP3 1 AP responses were often unusually high, and so these wells were excluded.

Without identifying underlying sources of variable responses, we normalized well-to-well differences by compensating based on infected cell density. A linear fit of the median GCaMP3 $\Delta F/F_0$ responses in wells as a function of number of infected cells was calculated for control wells from all plates. For screening, compensated response values of GCaMP3 variants were obtained by dividing raw values by values on this GCaMP3 standard curve according to density for each well (Figure 6D).

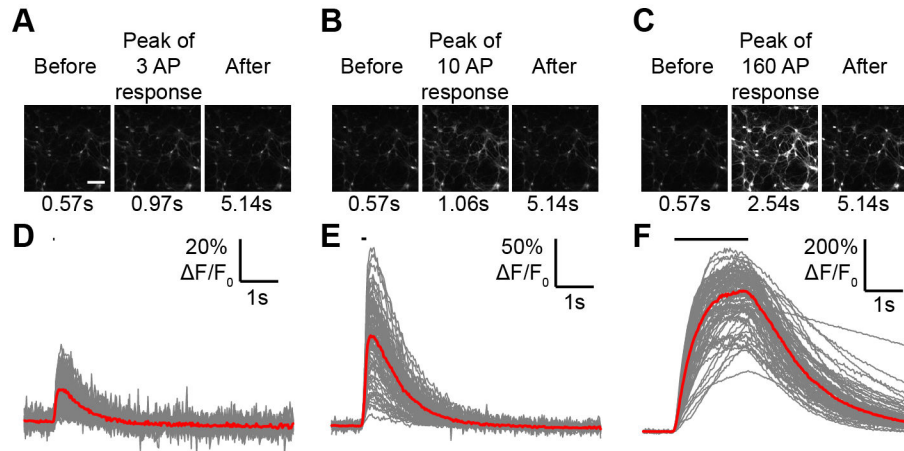


Figure 3. GCaMP3 fluorescence responses in neuronal culture. (A) 3 AP fluorescence response for GCaMP3. Scale bar: 150 μm . (B) 10 AP. (C) 160 AP. (D) 3 AP $\Delta F/F_0$ traces for 78 regions of interest (gray). Median trace (red). Stimulus duration (black line). (E) 10 AP. (F) 160 AP.

doi: 10.1371/journal.pone.0077728.g003

Platform detection sensitivity and throughput

We estimated the detection sensitivity of our assay for improvements over GCaMP3 performance by examining the distribution of GCaMP3 responses across wells. Using uncompensated data from 249 GCaMP3 wells, we selected random sets of 3, 4, 6, 8, 10, and 12 replicates 10^5 times to generate simulated distributions of GCaMP3 medians. The difference between the mean and the 99th percentile of these distributions normalized by the mean defined the detection sensitivity (for $\alpha=0.01$). Figure 6E shows the percent changes that would be detectable by the assay as a function of replicate number. Increasing replicate number made the assay more sensitive. The assay was less sensitive with low AP stimulation. For example, with 4 replicates, 280%, 156%, 78%, and 20% $\Delta F/F_0$ improvements over GCaMP3 could be detected for 1, 3, 10, and 160 AP stimulation, respectively (for $\alpha=0.01$). Additionally, 23% decay time improvements over GCaMP3 could be detected for 10 AP stimulation.

The same analysis was carried out using cell density compensated data (Figure 6F). Compensation improved sensitivity in the low AP range and with low replicates for $\Delta F/F_0$ measurements. With 4 replicates, 256%, 139%, 69%, and 20% $\Delta F/F_0$ improvements over GCaMP3 could be detected for 1, 3, 10, and 160 AP stimulation, respectively (for $\alpha=0.01$). For decay time, 25% improvements over GCaMP3 could be detected for 10 AP stimulation.

We also evaluated the sensitivity of our assay by imaging calcium indicators previously tested in a variety of assays [5,20,34]. For small numbers of action potentials, the response amplitudes for Fluo4 and GCaMP5G [20] were larger than for GCaMP3 (Figure 7A). Additionally, the fast rise time of Fluo4 was readily observed relative to GCaMP3 and GCaMP5G (Figure 7B).

We used the neuronal culture screening assay to find novel GCaMP6 indicators with improved sensitivity compared with GCaMP3 and GCaMP5G [34]. Indicator performance in the

screening assay generally correlated with performance in cortical neurons *in vivo* [5,20,34] (Figure 7C, linear regression, $R^2=0.54$, $F(1,3)=3.48$, $p=0.16$; Figure 7D, linear regression, $R^2=0.92$, $F(1,2)=23.99$, $p=0.04$).

Assay throughput was limited by the initial number of primary neurons prepared ($\sim 2.25 \times 10^5$ cells plated/well, average 41.6 regions of interest imaged/well) and the number of replicates tested for each GCaMP3 variant. Eight replicates/variant were routinely used in the screening assay, as described above (1, 2, 3, 5, 10, 20, 40, 80, 160 AP stimuli; 40 V, 83 Hz, 1 ms stimuli; intrastimulus interval ~ 20 s). With 8 replicates, estimated detectable improvements for uncompensated $\Delta F/F_0$ at 1, 3, 10, 160 AP, and decay time at 10 AP were: 134%, 108%, 60%, 15%, and 16%, respectively. For cell density compensated data, estimated detectable improvements were: 135%, 94%, 48%, 15%, and 17%, respectively. For 22.5×10^6 cells (from ~ 12 neonatal rat pups) and 8 replicates/variant, 24 variants were tested in 16 h of imaging time, and ~ 240 GB of image data were generated.

Comparison of GCaMP3 variant performance in neuronal culture versus solution

Our goal is to engineer protein indicators of neuronal function. How predictive are solution measurements with respect to calcium sensor sensitivity and kinetics in neurons? To address this question, we characterized mutated GCaMP3 variants in purified protein experiments and in the neuronal assay. Mutations in one of several GCaMP3 domains could affect peak fluorescence, F_0 , calcium affinity, and kinetics. We compared results from solution measurements with the neuronal assay (Figure 8).

For purified protein, we measured the maximal fluorescence change ($\Delta F_{\text{sat}}/F_{\text{apo}}$) and the apparent affinity for calcium (K_d) for several GCaMP3 variants. The peak response improvements for GCaMP5G were seen in both the neuronal and purified protein assays (Figure 8, Table S1). In general, larger

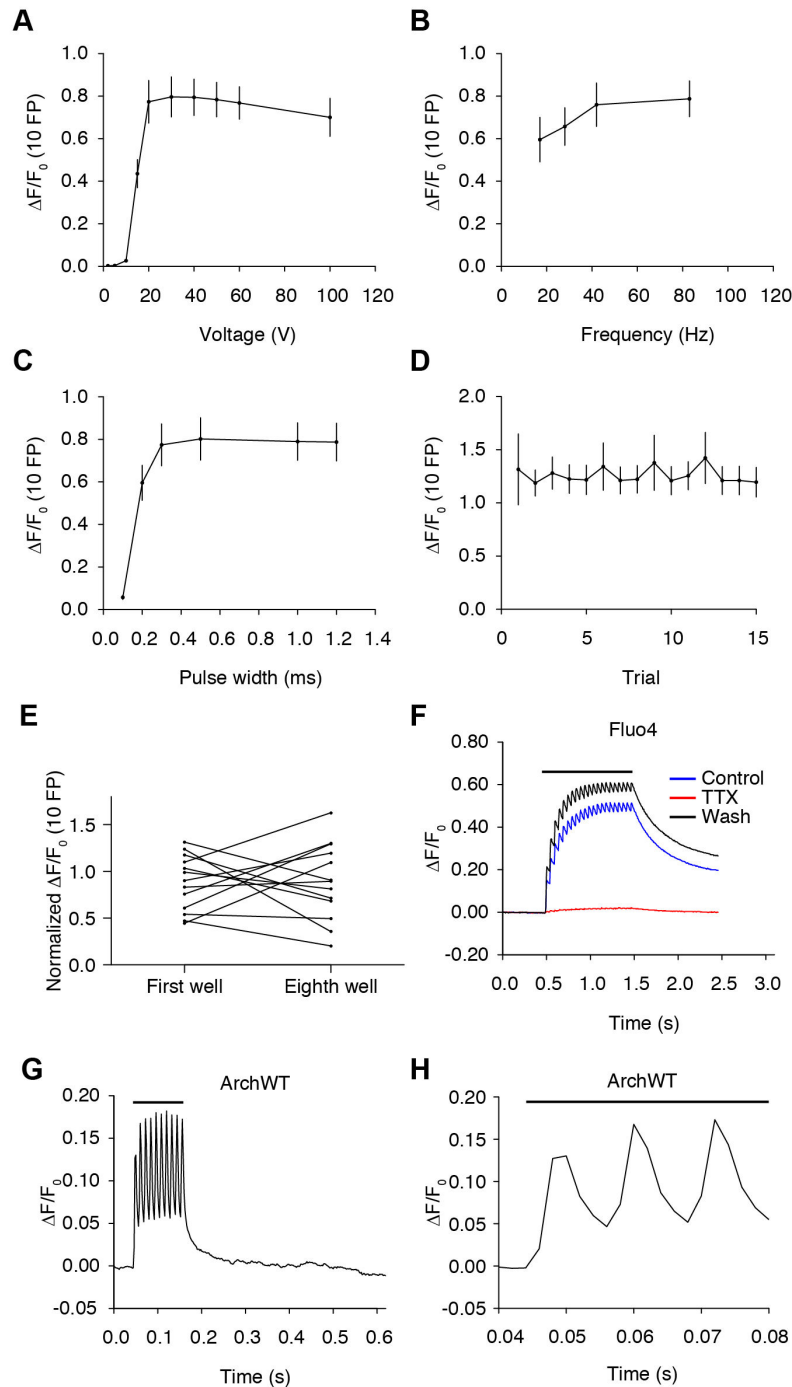


Figure 4. Optimization of platform stimulation parameters. (A) Voltage dependency of GCaMP3 $\Delta F/F_0$ (10 FP) response at 2, 5, 10, 15, 20, 30, 40, 50, 60, 100 V at 83 Hz and 1 ms pulse width (median \pm s.e.m.; 8 wells). (B) Frequency dependency at 17, 28, 42, 83 Hz at 40 V and 1 ms pulse width (8 wells). (C) Stimulus pulse width dependency at 0.1, 0.2, 0.3, 0.5, 1, 1.2 ms at 40 V and 83 Hz (8 wells). (D) Response to 15 separate trials with \sim 1-min intratrial intervals (40 V, 83 Hz, 1 ms pulse width; 26 wells). (E) $\Delta F/F_0$ (10 AP) responses of first and eighth wells on individual plates normalized to the averaged response of all eight wells. Stimulation of the first and last wells was separated by \sim 90 min (first and eighth wells from 13 plates). (F) Fluo4 averaged $\Delta F/F_0$ (21 AP) trace (6 regions of interest) in imaging buffer (blue), after addition of 1 μ M tetrodotoxin (TTX, red), and after washout (black). High-speed imaging was employed (227 Hz). Stimulus duration (black line). (G) Voltage imaging trace of neurons in a single well showing the $\Delta F/F_0$ (10 FP) response of the ArchWT-GFP voltage sensor at 40 V, 83 Hz, and 1 ms pulse width. Pixels were segmented for analysis based on activity [33]. (H) Voltage imaging from (G) on expanded timescale.

doi: 10.1371/journal.pone.0077728.g004

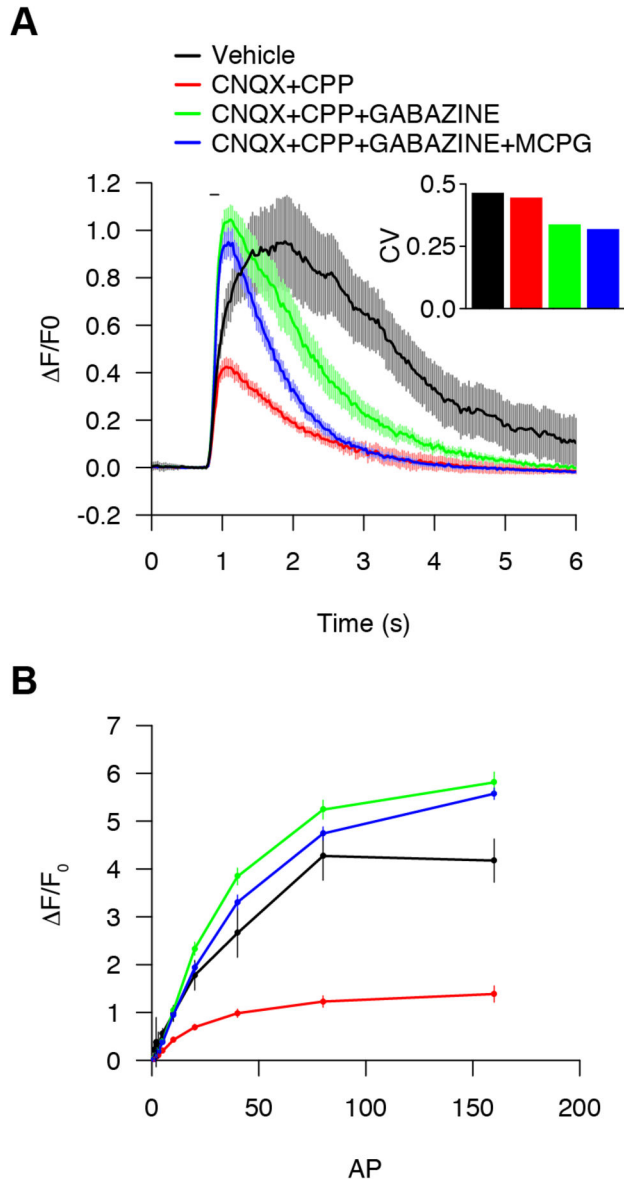


Figure 5. Optimization of platform pharmacological parameters. (A) $\Delta F/F_0$ (10 AP) response over time with imaging buffer alone (vehicle, black; 5 wells); ionotropic glutamate receptor blockers (CNQX+CPP, red; 30 wells); ionotropic glutamate and GABA receptor blockers (CNQX+CPP+GABAZINE, green; 28 wells); ionotropic glutamate, GABA, and metabotropic glutamate receptor blockers (CNQX+CPP+GABAZINE+MCPG, blue; 28 wells); (median \pm s.e.m.). (Inset) The coefficient of variation of peak responses. (B) $\Delta F/F_0$ responses from 1-160 AP (median \pm s.e.m.).

doi: 10.1371/journal.pone.0077728.g005

fluorescence changes in solution predicted larger fluorescence changes in neurons (Figure 8A, larger circles near top) and lower affinity implied faster response decay kinetics in neurons (Figure 8B, smaller circles on right). However, equilibrium solution measurements rarely predicted both the response

amplitudes and signal decay times for small trains of APs relevant to neurophysiology.

Discussion

Fluorescent protein sensors for neuronal activity are key reagents for dissecting neuronal circuit function [35-37]. Despite considerable effort, optimization of calcium indicator proteins has been slowed by development cycles that relied on testing in non-neuronal assays and then validating performance in neuronal systems. Here we developed a primary neuron-based screening platform to test sensors in the relevant context.

Other screening systems have been previously reported to image neuronal dynamics in response to trains of APs [25]. Our method is based on high-speed imaging with cellular resolution and is coupled to physiological stimulation of neural activity. Automated image segmentation and analysis allowed measurements from individual neurons, which increased the sensitivity of the assay. High-speed imaging allows optimization of sensors for speed. Similar image segmentation methods could be used to perform measurements on neuronal microcompartments, such as axons, presynaptic terminals, and dendritic spines. Simultaneous optimization of sensor sensitivity and kinetic parameters in neurons will be more efficient than solution-based methods for improving neuronal activity detectors. Because measurements in cultured neurons predict performance *in vivo* (Figure 7C,D), neuronal screening will greatly shorten the optimization cycle. This assay system could be adapted for optimization of sensors of virtually any neuronal state variable (e.g. calcium concentration, membrane voltage, extracellular neurotransmitter levels, intracellular signaling pathways) [33,38]. It also could be used for the optimization of effector proteins that perturb neuronal activity [39,40]. Finally, the assay is also suitable for dissection of the genetic pathways involved in controlling calcium and other neuronal variables that can be imaged with fluorescence microscopy.

Materials and Methods

Molecular biology

A third-generation, simian immunodeficiency (SIV) based, pro lentiviral vector was used [41]. Sequences containing a 476-bp human *synapsin-1* promoter element [26], GCaMP3 coding region [5], an encephalomyocarditis virus IRES, an nls fused to mCherry [27], and a woodchuck hepatitis post-transcriptional regulatory element (WPRE) were inserted between the pro lentiviral long terminal repeats (Figure 1B and S3). GCaMP3 variants were constructed by PCR of the coding region using mutagenic primers. Mutated coding regions were then inserted into the pro lentiviral vector by isothermal assembly [42].

Neuronal culture

Experiments were conducted according to National Institutes of Health guidelines for animal research and were approved by the Janelia Farm Research Campus Institutional Animal Care

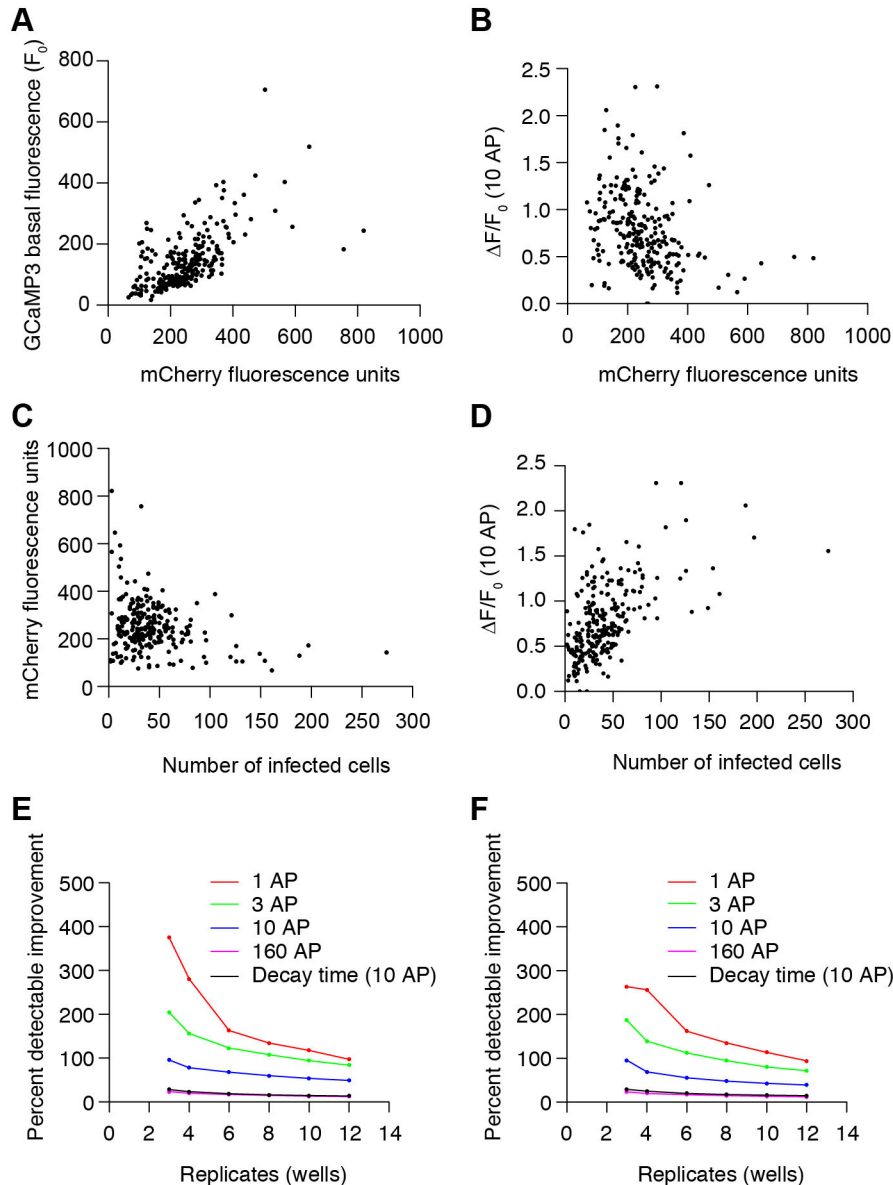


Figure 6. Neuronal culture platform performance parameters and detection sensitivity. (A) GCaMP3 basal fluorescence (F_0) relationship with mCherry fluorescence (249 wells). (B) $\Delta F/F_0$ (10 AP) response relationship with mCherry fluorescence. (C) mCherry fluorescence relationship with number of infected cells. (D) Median $\Delta F/F_0$ (10 AP) response dependency on number of infected cells. (E) Percent detectable improvement relative to GCaMP3 performance was estimated by simulating 10^5 experiments using 3 to 12 replicate wells drawn from a data set of 249 GCaMP3 wells. The difference between the mean and the 99th percentile of simulated result distributions normalized by the mean defined the detection sensitivity at $\alpha=0.01$ (red: 1 AP, green: 3 AP, blue: 10 AP, magenta: 160 AP, black: decay time (10 AP)). (F) After compensation correcting for infected cell density effect.

doi: 10.1371/journal.pone.0077728.g006

and Use Committee and Institutional Biosafety Committee. Neonatal rat pups were euthanized, and hippocampi were dissected and dissociated in papain (Worthington, ~12 U/hippocampal pair) in neural dissection solution (10 mM HEPES pH 7.4 in Hanks' Balanced Salt Solution) for 25 min at 37°C. Following trituration with a Pasteur pipette and passage through a 40- μ m strainer, cells were plated at a density of 2.25

$\times 10^5$ viable cells/well in 150 μ L plating medium (28 mM glucose, 2.4 mM NaHCO₃, 100 μ g/mL transferrin, 25 μ g/mL insulin, 2 mM L-glutamine, 100 U/mL penicillin, 10 μ g/mL streptomycin, 10% fetal bovine serum in MEM) in 24-well glass-bottom plates (Mattek, #1.5 glass cover slips). Wells were pre-coated with 100 μ L Matrigel (1:50 dilution in MEM, BD Biosciences), which was aspirated immediately before plating

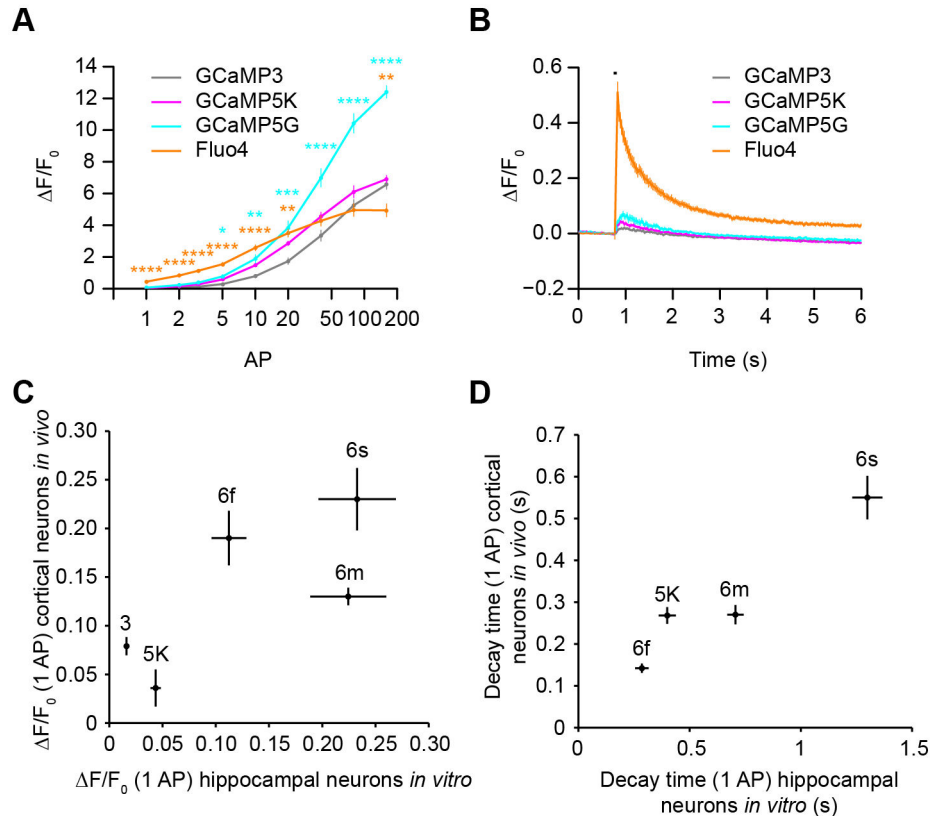


Figure 7. Calcium indicator performance *in vitro* and *in vivo*. (A) Median $\Delta F/F_0$ responses of GCaMP3 (gray, 6 wells), GCaMP5K (magenta, 6 wells), GCaMP5G (cyan, 6 wells), and Fluo4 (orange, 8 wells) after 1, 2, 3, 5, 10, 20, 40, 80, 160 AP (median \pm s.e.m.; * $p < 0.05$, ** $p < 0.01$, *** $p < 0.001$, **** $p < 0.0001$, compared to GCaMP3 by Tukey HSD test). (B) Averaged $\Delta F/F_0$ (1 AP) trace for GCaMP3 (6 wells), GCaMP5G (6 wells), and Fluo4 (8 wells). Stimulus duration (black line); (median \pm s.e.m.). (C) $\Delta F/F_0$ (1 AP) response of GCaMP3 (9 cells), GCaMP5K (9 cells), 6f (11 cells), 6m (10 cells), and 6s (9 cells) in mouse somatosensory (GCaMP3) or visual cortical neurons (GCaMP5K, 6f, 6m, 6s; data from [5,20,34]) versus neuronal culture (GCaMP3, 249 wells; 5K, 6 wells; 6f, 16 wells; 6m, 16 wells; 6s, 17 wells); (median \pm s.e.m.). (D) Decay times ($\tau_{1/2}$) for GCaMP5K, 6f, 6m, and 6s. GCaMP3 cortical decay time was not reported in [5].

doi: 10.1371/journal.pone.0077728.g007

cells. After 1 h at 37°C, 1 mL plating medium was added to wells. After 16 h, plating medium was replaced with 1 mL growth medium (28 mM glucose, 2.4 mM NaHCO₃, 100 μ g/mL transferrin, B-27 supplement (1X, Invitrogen), 500 μ M L-glutamine, 100 U/mL penicillin, 10 μ g/mL streptomycin, 5% fetal bovine serum in MEM).

Lentiviral particle production and infection

A pro lentiviral construct was combined with packaging and coat pseudotyping DNA constructs (pCAG-SIVgprre, pCAG4-RTR-SIV, pCMV-VSV-G) [41,43] and transfected into 32 x 10⁶ HEK293T/17 cells (ATCC) cultured in DMEM and 10% fetal bovine serum in 10-cm plates. After 72 h, supernatant was collected (6 mL) and passed through a 0.45- μ m filter. For each well of a 24-well plate, 0.5 mL of lentivirus was combined with 0.5 mL of conditioned growth medium and incubated for 18 h at 37°C. Medium was exchanged with 1 mL growth medium supplemented with 4 μ M AraC to inhibit glial proliferation. Lentiviral particles were used in a biosafety level 2 laboratory.

Sufficient virus (up to 4 mL) can also be produced in 6-well format (3.5-cm wells).

Stimulus and imaging

Neuronal culture growth medium was exchanged 3 times with imaging buffer (145 mM NaCl, 2.5 mM KCl, 10 mM glucose, 10 mM HEPES pH 7.4, 2 mM CaCl₂, 1 mM MgCl₂) and imaged in 500 μ L of imaging buffer and drugs (10 μ M CNQX, 10 μ M (R)-CPP, 10 μ M gabazine, 1 mM (S)-MCPG, Tocris). A Grass S48 Stimulator (Grass Technologies) was used for field stimulation. A digital routing control box coordinated stimulation with TTL signals during imaging. The microscope was an Olympus IX81 with 10X (0.4 NA) air objective lens, Prior H117 ProScan II motorized stage, Andor Technology EMCCD camera (DU897_BV, 512x512 resolution, 35 frames/s, 100 electron multiplying gain, 1X pre-amp gain, -60°C), Cairn OptoLED illumination system, and Chroma ET-GFP and ET-TxRed filter sets. For voltage imaging, a 60X (1.45 NA) oil objective lens, 638 nm laser illumination (100 mW

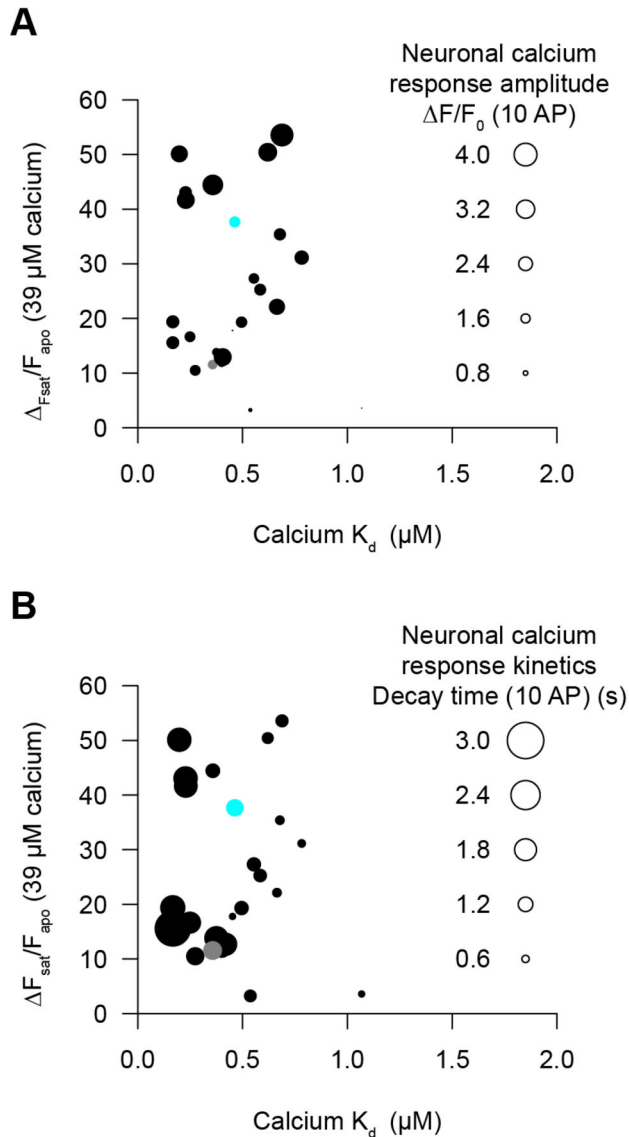


Figure 8. Neuronal culture platform and purified protein measurements for GCaMP variants. Purified protein measurements do not predict GCaMP variant performance in neurons. Each variant is represented as a circle. The calcium affinity and fluorescence response from purified protein measurements are plotted on the x-axis and y-axis, respectively. Variant performance in neurons (fluorescence change or decay kinetics) is shown by the area of each circle. **(A)** Neuronal $\Delta F/F_0$ (10 AP; 4 to 249 wells) of variants (circle area) compared with protein $\Delta F_{\text{sat}}/F_{\text{apo}}$ and apparent calcium affinity (K_d). **(B)** Neuronal decay time ($\tau_{1/2}$, 10 AP) of variants (circle area) compared with protein $\Delta F_{\text{sat}}/F_{\text{apo}}$ and apparent calcium affinity (K_d). GCaMP3 (gray circle), GCaMP5G (cyan circle).

doi: 10.1371/journal.pone.0077728.g008

DPSS laser, Crystalaser), and a high-speed Andor Technology EMCCD camera (DU860_BV, 128x128 resolution, 500

frames/s, 1000 electron multiplying gain, 1X pre-amp gain, -60°C) were used. The imaging system was controlled by custom journals written in MetaMorph software (version 7.7.5, Molecular Devices), which controlled data acquisition boards (USB-6501, USB-9263, National Instruments). The stimulation and image timing was controlled as a slave using another data acquisition board (USB-6259, National Instruments) and Ephus software [30]. The imaging computer was from PSSC Labs (PowerStation Duo I2600, dual Intel X5650 Hex Core 2.66 Ghz processors, 96 GB RAM).

Image analysis

Analysis was implemented in MATLAB (release 2010a, MathWorks). The neuronal cell body segmentation strategy was to fit a circle of fixed radius around pixels to find centers of greatest mCherry fluorescence above a defined threshold. Center locations were used to construct Voronoi subregions [31]. Center locations were then used to draw circles of greatest GCaMP fluorescence above threshold within subregions. Circles were shrunk to exclude the lowest fluorescence quartile and holes were filled to define regions of interest. Regions of interest were excluded that contacted the image boundary. For GCaMP fluorescence transients, background subtraction was applied through subtraction of the mean of the lowest 5% intensity values. F_0 was defined as the mean of fluorescence 1 s prior to stimulus onset.

Calcium titrations of purified proteins

pRSET-A plasmids containing GCaMP variants were used to express protein in T7 Express *E. coli* cells (New England Biolabs) using 100 mL of ZYM-5052 autoinduction media [44] and ampicillin at 30°C for 48 h. Pelleted cells were lysed in B-PER (Thermo Scientific), 1 mg/mL lysozyme, and 15 U/mL DNase at 22°C for 30 min. After clearing by centrifugation, variants were purified using nickel-charged Profinity IMAC resin (Bio-Rad). Columns were washed with 20 mM Tris pH 8.0, 300 mM NaCl, 1 mM imidazole and then with 20 mM Tris pH 8.0, 500 mM NaCl, 10 mM imidazole. Variants were eluted in 20 mM Tris pH 8.0, 100 mM NaCl, 100 mM imidazole. Eluted protein concentrations ranged from 9-67 μM . Eleven-point calcium titrations were done using EGTA-buffered calcium solutions, similar to the protocol of the Calcium Calibration Buffer Kit #1 (Life Technologies). Green fluorescence intensities (excitation 485 nm, 5 nm bandpass; emission 510 nm, 5 nm bandpass) were measured using a Safire2 plate reader (Tecan). Apparent calcium affinity (K_d) was calculated from the inflection point of a sigmoidal fit to the fluorescence intensities.

Supporting Information

Figure S1. Voltage imaging with the ArchWT-GFP voltage sensor. **(A-D)** Median $\Delta F/F_0$ (10 FP) traces of ArchWT-GFP voltage sensor fluorescence showing frequency dependency at 17, 28, 42, 83 Hz at 40 V and 1 ms pulse width from a single well. **(E-J)** Stimulus pulse width dependency at 0.1, 0.2, 0.3, 0.5, 1, 1.2 ms at 40 V and 83 Hz. **(K-T)** Voltage dependency at

2, 5, 10, 15, 20, 30, 40, 50, 60, 100 V at 83 Hz and 1 ms pulse width. (U-W) Stability of neuronal responses over 3 trials with ~1-min intratrial intervals.
(TIF)

Figure S2. Effects of neuronal clumping on GCaMP3 responses. (A-C) Morphology and responses of unclumped neurons. Scale bar: 150 μ m. (D-F) Clumped neurons. (A,D) GCaMP3 fluorescence and bright field images. (B,E) $\Delta F/F_0$ response map for GCaMP3 for 1, 10, 160 AP (red: high response, blue: low response). (C,F) 1, 10, 160 AP $\Delta F/F_0$ traces for regions of interest (gray). Median trace (red).
(TIF)

Figure S3. Plasmid map and sequence of lentiviral expression vector.
(PDF)

Table S1. GCaMP3 variant calcium-induced fluorescence changes and calcium affinity measured from purified proteins and action potential-induced fluorescence changes and decay kinetics measured in neurons.

References

- Looger LL, Griesbeck O (2012) Genetically encoded neural activity indicators. *Curr Opin Neurobiol* 22: 18-23. doi:10.1016/j.conb.2011.10.024. PubMed: 22104761.
- Horikawa K, Yamada Y, Matsuda T, Kobayashi K, Hashimoto M et al. (2010) Spontaneous network activity visualized by ultrasensitive Ca(2+) indicators, yellow Cameleon-Nano. *Nat Methods* 7: 729-732. doi: 10.1038/nmeth.1488. PubMed: 20693999.
- Huber D, Gutnisky DA, Peron S, O'Connor DH, Wiegert JS et al. (2012) Multiple dynamic representations in the motor cortex during sensorimotor learning. *Nature* 484: 473-478. doi:10.1038/nature11039. PubMed: 22538608.
- Mank M, Santos AF, Drenth S, Mrcic-Flogel TD, Hofer SB et al. (2008) A genetically encoded calcium indicator for chronic in vivo two-photon imaging. *Nat Methods* 5: 805-811. doi:10.1038/nmeth.1243. PubMed: 19160515.
- Tian L, Hires SA, Mao T, Huber D, Chiappe ME et al. (2009) Imaging neural activity in worms, flies and mice with improved GCaMP calcium indicators. *Nat Methods* 6: 875-881. doi:10.1038/nmeth.1398. PubMed: 19898485.
- Kerr R, Lev-Ram V, Baird G, Vincent P, Tsien RY et al. (2000) Optical imaging of calcium transients in neurons and pharyngeal muscle of *C. elegans*. *Neuron* 26: 583-594. doi:10.1016/S0896-6273(00)81196-4. PubMed: 10896155.
- Mao T, O'Connor DH, Scheuss V, Nakai J, Svoboda K (2008) Characterization and subcellular targeting of GCaMP-type genetically encoded calcium indicators. *PLoS ONE* 3: e1796. doi:10.1371/journal.pone.0001796. PubMed: 18350138.
- Petreaanu L, Gutnisky DA, Huber D, Xu NL, O'Connor DH et al. (2012) Activity in motor-sensory projections reveals distributed coding in somatosensation. *Nature* 489: 299-303. doi:10.1038/nature11321. PubMed: 22922646.
- Dreosti E, Odermatt B, Dorostkar MM, Lagnado L (2009) A genetically encoded reporter of synaptic activity in vivo. *Nat Methods* 6: 883-889. doi:10.1038/nmeth.1399. PubMed: 19898484.
- Luo L, Callaway EM, Svoboda K (2008) Genetic dissection of neural circuits. *Neuron* 57: 634-660. doi:10.1016/j.neuron.2008.01.002. PubMed: 18341986.
- Miyawaki A, Llopis J, Heim R, McCaffery JM, Adams JA et al. (1997) Fluorescent indicators for Ca²⁺ based on green fluorescent proteins and calmodulin. *Nature* 388: 882-887. doi:10.1038/42264. PubMed: 9278050.
- Zariwala HA, Borghuis BG, Hoogland TM, Madisen L, Tian L et al. (2012) A Cre-Dependent GCaMP3 Reporter Mouse for Neuronal Imaging In Vivo. *J Neurosci* 32: 3131-3141. doi:10.1523/JNEUROSCI.4469-11.2012. PubMed: 22378886.
- Helmchen F, Imoto K, Sakmann B (1996) Ca²⁺ buffering and action potential-evoked Ca²⁺ signaling in dendrites of pyramidal neurons. *Biophys J* 70: 1069-1081. doi:10.1016/S0006-3495(96)79653-4. PubMed: 8789126.
- Maravall M, Mainen ZM, Sabatini BL, Svoboda K (2000) Estimating intracellular calcium concentrations and buffering without wavelength ratioing. *Biophys J* 78: 2655-2667. doi:10.1016/S0006-3495(00)76809-3. PubMed: 10777761.
- Sabatini BL, Oertner TG, Svoboda K (2002) The life cycle of Ca(2+) ions in dendritic spines. *Neuron* 33: 439-452. doi:10.1016/S0896-6273(02)00573-1. PubMed: 11832230.
- Cox CL, Denk W, Tank DW, Svoboda K (2000) Action potentials reliably invade axonal arbors of rat neocortical neurons. *Proc Natl Acad Sci U S A* 97: 9724-9728. doi:10.1073/pnas.170278697. PubMed: 10931955.
- Berridge MJ, Bootman MD, Roderick HL (2003) Calcium signalling: dynamics, homeostasis and remodelling. *Nat Rev Mol Cell Biol* 4: 517-529. doi:10.1038/nrm1155. PubMed: 12838335.
- Nakai J, Ohkura M, Imoto K (2001) A high signal-to-noise Ca(2+) probe composed of a single green fluorescent protein. *Nat Biotechnol* 19: 137-141. doi:10.1038/84397. PubMed: 11175727.
- Zhao Y, Araki S, Wu J, Teramoto T, Chang YF et al. (2011) An expanded palette of genetically encoded Ca(2+) indicators. *Science* 333: 1888-1891. doi:10.1126/science.1208592. PubMed: 21903779.
- Akerboom J, Chen TW, Wardill TJ, Tian L, Marvin JS et al. (2012) Optimization of a GCaMP Calcium Indicator for Neural Activity Imaging. *J Neurosci* 32: 13819-13840. doi:10.1523/JNEUROSCI.2601-12.2012. PubMed: 23035093.
- Pologruto TA, Yasuda R, Svoboda K (2004) Monitoring neural activity and [Ca²⁺] with genetically encoded Ca²⁺ indicators. *J Neurosci* 24: 9572-9579. doi:10.1523/JNEUROSCI.2854-04.2004. PubMed: 15509744.
- Ohkura M, Sasaki T, Kobayashi C, Ikegaya Y, Nakai J (2012) An improved genetically encoded red fluorescent Ca²⁺ indicator for detecting optically evoked action potentials. *PLoS ONE* 7: e39933. doi: 10.1371/journal.pone.0039933. PubMed: 22808076.
- Reiff DF, Ihring A, Guerrero G, Isacoff EY, Joesch M et al. (2005) In vivo performance of genetically encoded indicators of neural activity in flies. *J Neurosci* 25: 4766-4778. doi:10.1523/JNEUROSCI.4900-04.2005. PubMed: 15888652.
- Muto A, Ohkura M, Kotani T, Higashijima S, Nakai J et al. (2011) Genetic visualization with an improved GCaMP calcium indicator reveals spatiotemporal activation of the spinal motor neurons in zebrafish. *Proc Natl Acad Sci U S A* 108: 5425-5430. doi:10.1073/pnas.1000887108. PubMed: 21383146.

25. Hempel CM, Sivula M, Levenson JM, Rose DM, Li B et al. (2011) A system for performing high throughput assays of synaptic function. *PLOS ONE* 6: e25999. doi:10.1371/journal.pone.0025999. PubMed: 21998743.
26. Kügler S, Meyn L, Holzmüller H, Gerhardt E, Isenmann S et al. (2001) Neuron-specific expression of therapeutic proteins: evaluation of different cellular promoters in recombinant adenoviral vectors. *Mol Cell Neurosci* 17: 78-96. doi:10.1006/mcne.2000.0929. PubMed: 11161471.
27. Shaner NC, Campbell RE, Steinbach PA, Giepmans BN, Palmer AE et al. (2004) Improved monomeric red, orange and yellow fluorescent proteins derived from *Discosoma* sp. red fluorescent protein. *Nat Biotechnol* 22: 1567-1572. doi:10.1038/nbt1037. PubMed: 15558047.
28. Basarsky TA, Parpura V, Haydon PG (1994) Hippocampal synaptogenesis in cell culture: developmental time course of synapse formation, calcium influx, and synaptic protein distribution. *J Neurosci* 14: 6402-6411. PubMed: 7965045.
29. Brenner JF, Dew BS, Horton JB, King T, Neurath PW et al. (1976) An automated microscope for cytologic research a preliminary evaluation. *J Histochem Cytochem* 24: 100-111. doi:10.1177/24.1.1254907. PubMed: 1254907.
30. Suter BA, O'Connor T, Iyer V, Petreanu LT, Hooks BM et al. (2010) Ephus: multipurpose data acquisition software for neuroscience experiments. *Front Neural Circuits* 4: 100. PubMed: 21960959.
31. Jones TR, Carpenter A, Golland P (2005) Voronoi-based segmentation of cells on image manifolds. *Computer Vision Biomedical Images Applications Proc* 3765: 535-543. doi:10.1007/11569541_54.
32. Ryan TA, Smith SJ (1995) Vesicle pool mobilization during action potential firing at hippocampal synapses. *Neuron* 14: 983-989. doi:10.1016/0896-6273(95)90336-4. PubMed: 7748565.
33. Kralj JM, Douglass AD, Hochbaum DR, Maclaurin D, Cohen AE (2012) Optical recording of action potentials in mammalian neurons using a microbial rhodopsin. *Nat Methods* 9: 90-95. doi:10.1038/nchembio.1135. PubMed: 22120467.
34. Chen TW, Wardill TJ, Sun Y, Pulver SR, Renninger SL et al. (2013) Ultra-sensitive fluorescent proteins for imaging neuronal activity. *Nature* 499: 295-300. doi:10.1038/nature12354. PubMed: 23868258.
35. Wang Y, Guo HF, Pologruto TA, Hannan F, Hakker I et al. (2004) Stereotyped odor-evoked activity in the mushroom body of *Drosophila* revealed by green fluorescent protein-based Ca²⁺ imaging. *J Neurosci* 24: 6507-6514. doi:10.1523/JNEUROSCI.3727-03.2004. PubMed: 15269261.
36. Ng M, Roorda RD, Lima SQ, Zemelman BV, Morcillo P et al. (2002) Transmission of olfactory information between three populations of neurons in the antennal lobe of the fly. *Neuron* 36: 463-474. doi:10.1016/S0896-6273(02)00975-3. PubMed: 12408848.
37. Bozza T, McGann JP, Mombaerts P, Wachowiak M (2004) In vivo imaging of neuronal activity by targeted expression of a genetically encoded probe in the mouse. *Neuron* 42: 9-21. doi:10.1016/S0896-6273(04)00144-8. PubMed: 15066261.
38. Marvin JS, Borghuis BG, Tian L, Cichon J, Harnett MT et al. (2013) An optimized fluorescent probe for visualizing glutamate neurotransmission. *Nat Methods* 10: 162-170. doi:10.1038/nmeth.2333. PubMed: 23314171.
39. Nagel G, Szellas T, Huhn W, Kateriya S, Adeishvili N et al. (2003) Channelrhodopsin-2, a directly light-gated cation-selective membrane channel. *Proc Natl Acad Sci U S A* 100: 13940-13945. doi:10.1073/pnas.1936192100. PubMed: 14615590.
40. Han X, Boyden ES (2007) Multiple-color optical activation, silencing, and desynchronization of neural activity, with single-spike temporal resolution. *PLOS ONE* 2: e299. doi:10.1371/journal.pone.0000299. PubMed: 17375185.
41. Hanawa H, Hematti P, Keyvanfar K, Metzger ME, Krouse A et al. (2004) Efficient gene transfer into rhesus repopulating hematopoietic stem cells using a simian immunodeficiency virus-based lentiviral vector system. *Blood* 103: 4062-4069. doi:10.1182/blood-2004-01-0045. PubMed: 14976042.
42. Gibson DG, Young L, Chuang RY, Venter JC, Hutchison CA 3rd et al. (2009) Enzymatic assembly of DNA molecules up to several hundred kilobases. *Nat Methods* 6: 343-345. doi:10.1038/nmeth.1318. PubMed: 19363495.
43. Stewart SA, Dykxhoorn DM, Palliser D, Mizuno H, Yu EY et al. (2003) Lentivirus-delivered stable gene silencing by RNAi in primary cells. *RNA* 9: 493-501. doi:10.1261/rna.2192803. PubMed: 12649500.
44. Studier FW (2005) Protein production by auto-induction in high density shaking cultures. *Protein Expr Purif* 41: 207-234. doi:10.1016/j.pep.2005.01.016. PubMed: 15915565.